INTERNATIONAL JOURNAL FOR NUMERICAL METHODS IN FLUIDS, VOL. 8, 869–895 (1988)

SOME FAST 3D FINITE ELEMENT SOLVERS FOR THE GENERALIZED STOKES PROBLEM

J. CAHOUET AND J.-P. CHABARD

Laboratoire National d'Hydraulique, Electricite de France, 6 quai Watier, 78401 Chatou Cedex, France

SUMMARY

This paper is devoted to a comparison of various iterative solvers for the Stokes problem, based on the preconditioned Uzawa approach. In the first section the basic equations and general results of gradient-like methods are recalled. Then a new class of preconditioners, whose optimality will be shown, is introduced. In the last section numerical experiments and comparisons with multigrid methods prove the quality of these schemes, whose discretization is detailed.

KEY WORDS 3D Stokes problem Mixed finite element methods Primitive variables Gradient methods Convergence analysis

INTRODUCTION

The need to numerically solve the generalized Stokes problem (GSP) appears in incompressible fluid dynamics and in structural mechanics problems such as plasticity, beam and shell studies, etc.[1] Underlying any formulation of the Navier–Stokes equations, the GSP can be seen as a vital substep in the resolution of non-linear simulations, including non-Newtonian flows, combustion phenomena and turbulence modelling.[2] Moreover, such formulations can easily be transposed to weakly compressible media, permitting also a refined modelization of tides and storm surges through St Venant's (shallow water) equations.[3–5] To solve them, a wide diversity of numerical methods can be found in the literature.[6] Nevertheless, as they are often developed for very special situations, few schemes allow the treatment of industrial problems, whose main characteristics are:

(i) 3D flows in very complicated geometries (see Figure 1 for example)
(ii) basic equations coupled with complementary modelling (thermal buoyancy effects, turbulence, etc.)
(iii) various boundary conditions such as constrained velocities or stresses, symmetry and periodicity, wall treatment assuming logarithmic profiles,[7] etc.
(iv) robustness and simplicity of the algorithms (with no parameter to tune)
(v) efficiency and accuracy (a good mass balance is fundamental), with reasonable CPU costs and memory requirements.

Following Peyret and Taylor,[8] it seems that only the finite element (or finite volume) approach formulated in primitive variables (i.e. velocity and pressure) allows us to satisfy these various requirements.

Within that scope, this paper is devoted to a comparison of various iterative solvers based on

0271–2091/88/080869–27$13.50

Received 14 February 1987
Revised 16 September 1987

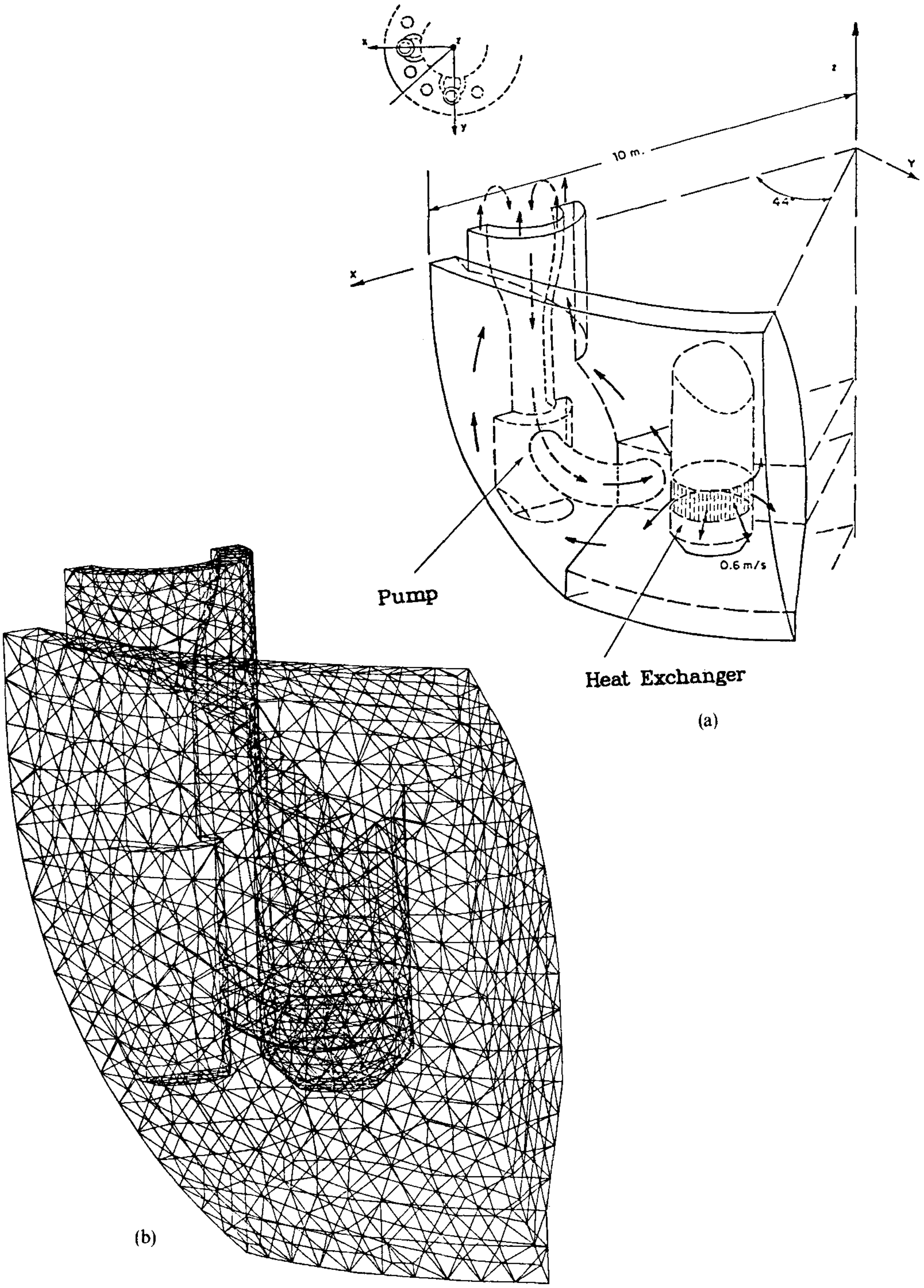

Figure 1. Example of industrial application. (a) Sketch of the cold plenum of a fast breeder reactor. (b) Finite element mesh of the cold plenum: 12936 P_1–P_2 tetrahedra, 20108 velocity nodes and 2896 pressure nodes

the preconditioned Uzawa approach. In the first section the basic equations and general results of gradient-like methods are recalled. Then a comparative analysis of classical improvements leads us to introduce a new class of preconditioners whose optimality will be shown. In the last section numerical experiments and comparisons with multigrid methods prove the quality of these schemes, whose discretization is detailed. Finally a three-dimensional turbulent simulation of the flow in a fast breeder reactor is briefly discussed and is shown to confirm the industrial adequacy of these schemes.

A GENERALIZED STOKES PROBLEM AND CLASSICAL GRADIENT METHODS

A generalized Stokes problem

The Stokes equations describe the motion of an incompressible viscous flow at very low Reynolds numbers. They can be written in a dimensionless form as

$$\nabla\cdot\mathbf{v}=0, \tag{1a}$$

$$\frac{\partial\mathbf{v}}{\partial t}-\frac{1}{Re}\nabla^2\mathbf{v}+\nabla P=\mathbf{s}. \tag{1b}$$

Here $\mathbf{v}$ and P denote respectively the velocity and the kinematic pressure field defined on a domain $\Omega(\Omega\subset\mathbb{R}^3)$ bounded by the boundary Γ, $\mathbf{s}$ describes the internal force per unit volume and Re denotes the Reynolds number, defined as

$$Re=\rho UL/\mu, \tag{2}$$

where ρ is the density, L a reference length, U a reference velocity and μ the dynamic viscosity.

The above equations are based on the Eulerian approach to the Navier–Stokes equations, neglecting non-linear terms; equations (1a) and (1b) express the mass balance and momentum balance respectively. The classical boundary value problem associated with this model is defined by:

(i) an initial distribution of velocity on Ω
(ii) the value of $\mathbf{v}$ on Γ at each time satisfying a zero-flux condition resulting from incompressibility:

$$\int_\Gamma \mathbf{v}\cdot\mathbf{n}\,\mathrm{d}\Omega=0. \tag{3}$$

Then we are able to introduce the discretization with respect to time. Choosing a time step $\mathrm{D}T$ and assuming that velocity $\mathbf{v}^n$ and pressure P^n at time $T^n=n\mathrm{D}T$ are known, many approaches have been studied to compute $\mathbf{v}^{n+1}$ and P^{n+1} at time $T+\mathrm{D}T$. Most of them lead to the same kind of elliptic problem—the so-called generalized Stokes problem or GSP. Indeed implicit schemes are generally chosen to avoid such a time step limitation as a parabolic stability criterion. Therefore time derivatives are discretized as

$$\partial\mathbf{v}/\partial t=\alpha\mathbf{v}^{n+1}-f(\mathbf{v}^n,\mathbf{v}^{n-1},\ldots) \tag{4}$$

and space derivatives as

$$\nabla^2\mathbf{v}=\theta\nabla^2\mathbf{v}^{n+1}-g(\mathbf{v}^n,\mathbf{v}^{n-1},\ldots), \tag{5}$$

$$\nabla P=\theta'\nabla P^{n+1}-h(P^n,P^{n-1},\ldots), \tag{6}$$

where f, g and h denote some simple linear functions taking into account the previous values of $\mathbf{v}$ and P.

For instance, the simplest first-order scheme ($\sim O(\mathrm{D}T)$) is the backward Euler implicit scheme

$$\nabla\cdot\mathbf{v}^{n+1}=0, \tag{7a}$$

$$\frac{1}{\mathrm{D}T}\mathbf{v}^{n+1}-\frac{1}{Re}\nabla^2\mathbf{v}^{n+1}+\nabla P^{n+1}=\frac{1}{\mathrm{D}T}\mathbf{v}^n+\mathbf{s}^n, \tag{7b}$$

equivalent to

$$\alpha=1/\mathrm{D}T,\qquad \theta=\theta'=1,\qquad f(\mathbf{v})=\alpha\mathbf{v},\qquad g=h=0. \tag{8}$$

Second-order schemes ($\sim O(\mathrm{D}T^2)$) are easily built by using a classical Crank–Nicholson approximation, i.e.

$$\alpha=2/\mathrm{D}T,\qquad \theta=\theta'=\tfrac{1}{2}, \tag{9}$$

as in Cahouet.[9]

Moreover, the same kind of GSP (with different values for α, θ) also appears as a fundamental substep in a wide variety of Navier–Stokes solvers using fractional step methods,[10,11] alternating direction methods[12,13] or least-squares conjugate gradient solutions.[14,15] All these approaches can be summarized in a general GSP framework as follows:

$$\left.\begin{array}{l}\text{Find } (\mathbf{v}, P) \text{ such that}\\ \nabla\cdot\mathbf{v}=0 \quad \text{over } \Omega,\\ \alpha\mathbf{v}-\nu\nabla^2\mathbf{v}+\nabla P=\mathbf{f} \text{ over } \Omega,\\ \text{with } \mathbf{v}=\mathbf{0} \quad \text{on } \Gamma,\\ \qquad \mathbf{s} \text{ given on } \Omega,\\ \qquad (\alpha,\nu)\in\mathbb{R}^+\times\mathbb{R}^+_*.\end{array}\right\} \tag{10}$$

At this stage, a few points have to be emphasized:

(i) The main difficulties in solving this set of equations result from the presence of the linear constraint applied to $\mathbf{v}$ and from the lack of boundary conditions for the pressure.

(ii) The classical steady Stokes problem is related to $\alpha=0$.

(iii) For the sake of simplicity we choose, as usual, $\mathbf{v}$ equal to zero on Γ. However, non-homogeneous problems can also be written in the previous form by subtracting in equation (10) a velocity field satisfying

$$\begin{array}{ll}\nabla\cdot\mathbf{v}_0=0 & \text{over } \Omega\\ \mathbf{v}_0=\mathbf{v}_\Gamma & \text{on } \Gamma.\end{array} \tag{11}$$

The existence of $\mathbf{v}_0$ requires that $\mathbf{v}_\Gamma$ and Γ are sufficiently smooth. Thus the deviation between $\mathbf{v}$ and the exact unknown solution satisfies a homogeneous GSP with the modified right-hand side

$$\mathbf{f}'=\mathbf{f}-\alpha\mathbf{v}_0+\nu\nabla^2\mathbf{v}_0. \tag{12}$$

To conclude this presentation, we recall existence, uniqueness and regularity properties for the solution of the GSP. The main ideas underlying the proofs can be found in Cahouet and Hauguel,[16] but one can refer to Girault and Raviart[17] or Temam[13] for a complete description of functional spaces and proofs of theorems.

Theorem 1. Let Ω be a bounded and connected subset of $\mathbb{R}^N$ ($N=2, 3$) with a Lipschitz continuous boundary Γ and let $\mathbf{f}$ be a given function of $H^{-1}(\Omega)^N$; then there exists one and only one pair of functions $(\mathbf{v}, P)\in H_0^1(\Omega)^N\times L_0^2(\Omega)$ satisfying equation (10). If the constrained velocity on Γ belongs to $H^{1/2}(\Gamma)$, the result still holds with $\mathbf{v}$ in $H^1(\Omega)$.

This fundamental result requires a few comments about the pressure field which appears to belong to $L_0^2(\Omega)$.

(i) The subscript '0' recalls that the pressure is defined up to a constant and indefiniteness is avoided by choosing its mean value equal to zero. This constraint should be kept in mind and carefully discretized as explained in the Appendix;

(ii) One can be disappointed by the poor *a priori* regularity of the pressure. The origin of these restrictions, which can prohibit the use of some solvers (assuming P in $H^1(\Omega)$ for example), is clearly circumscribed by the following theorem (part (1) is proved in Temam[13] and part (2) in Grisvard[18]).

Theorem 2. (1) In addition to the hypothesis of Theorem 1, suppose that Γ is of class C^2 and $\mathbf{f}$ is given in $L^r(\Omega)$ for $1\leqslant r\leqslant 2$. Then the GSP has a unique solution $(\mathbf{v}, P)$ in $W^{2,N}(\Omega)\times W^{1,N}(\Omega)\times L_0^2(\Omega)$ and there exists a constant C_r independent of $(\mathbf{v}, P)$ and $\mathbf{f}$ such that

$$\|\mathbf{v}\|_{2,r}+\|P\|_{1,r}\leqslant C_r\|\mathbf{f}\|_{0,r}. \tag{13}$$

(2) When Γ is only Lipschitz continuous, this conclusion is still valid provided $N=2$ and Ω is convex.

As a conclusion (and in a less mathematical form), pressure regularity is related to:

(i) The regularity of $\mathbf{f}$, which is always satisfied in practice except for some thermal hydraulics studies where the Boussinesq approximation generates a non-smooth right-hand side (see the examples in Goussebaile and Jacomy[19]).

(ii) The regularity of $\mathbf{v}_\Gamma$ if non-homogeneous; Figure 2 illustrates two classical cases where $\mathbf{v}_\Gamma$ does not belong to the correct functional space.

(iii) The regularity of the boundary Γ: as for harmonic or biharmonic equations, the presence of a corner coupled or not with point (i) and (ii) may introduce local singularities. A fine description of these can be found in Bernardi and Raugel[20] for the 2D cases. We just recall that they look like

$$S(r,\theta)=r^{\mu}\quad(\mu\leqslant 0) \tag{14}$$

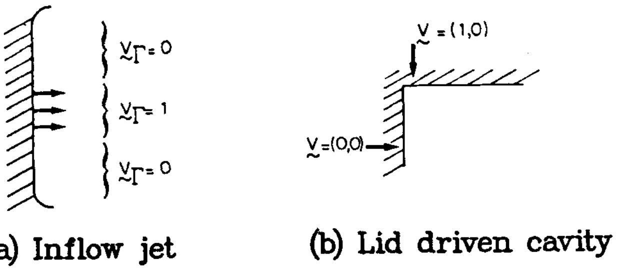
$\underset{\sim}{V}_\Gamma=0$
$\underset{\sim}{V}_\Gamma=1$
$\underset{\sim}{V}_\Gamma=0$
$\underset{\sim}{V}=(1,0)$
$\underset{\sim}{V}=(0,0)$

(a) Inflow jet

(b) Lid driven cavity

Figure 2. Irregular boundary conditions introducing singularities in the pressure field. (a) Inflow jet. (b) Lid driven cavity

in polar co-ordinates, with μ varying with respect to the value of the corner angle ω, and that they appear only if ω is strictly greater than $\pi/2$ (the singularity of the driven cavity test being related to point (ii) as in Serre[21]). For the 3D case some preliminary results have been recently presented by Grisvard.[22]

This basic information must be kept in mind for any FE approach to the GSP in order to choose an optimal mesh refined near singularities, an optimal solver compatible with pressure regularity and finally an optimal predictor for iterative schemes taking into account the irregular part of the field.

Uzawa algorithm

As explained before, many schemes are available to solve the GSP,[6] but the simplest approach is undoubtedly the iterative Uzawa algorithm, derived from an equivalent saddle-point approach of (1), defined as:

$$\left.\begin{aligned}
&\text{Find } \mathbf{u}\in H_0^1(\Omega)^N \text{ such that}\\
&\mathbf{u}=\min_{\mathbf{v}\in H_0^1(\Omega)^N}\ \max_{q\in L^2(\Omega)} \mathscr{L}_1(\mathbf{v},q), && \text{(15a)}\\
&\mathscr{L}_1(\mathbf{v},q)=\tfrac{1}{2}a(\mathbf{v},\mathbf{v})-(q,\nabla\cdot\mathbf{v})-(\mathbf{f},\mathbf{v}), && \text{(15b)}\\
&a(\mathbf{v},\mathbf{w})=\int_\Omega \alpha\mathbf{v}\cdot\mathbf{w}\,\mathrm{d}\Omega+\nu\int_\Omega \nabla\mathbf{v}\cdot\nabla\mathbf{w}\,\mathrm{d}\Omega. && \text{(15c)}
\end{aligned}\right\}$$

This algorithm, which is in fact a simple gradient method applied to the minimization of the dual functional,[23] is described as follows:

Step 0. Initialize P^n, $n=0$ (e.g. $P=0$).

Step 1. Compute the velocity associated to P^n by equation (1b), i.e.

$$\alpha\mathbf{v}^n-\nu\nabla^2\mathbf{v}^n=-\nabla P^n+\mathbf{s}, \tag{16}$$

with $\mathbf{v}^n=\mathbf{v}_\Gamma$ on Γ.

Step 2. Compute the divergence of $\mathbf{v}^n$.

Step 3. If the residual divergence vanishes, then $(\mathbf{v}^n, P^n)$ is the required solution; else define a new pressure field P^{n+1} as

$$P^{n+1}=P^n-\rho\nabla\cdot\mathbf{v}^n \tag{17}$$

and return to Step 1.

Convergence is proved for any ρ sufficiently small. This approach clearly exhibits the strong relationship which couples the divergence-free constraint and the pressure which appears as a Lagrange multiplier. More precisely, the two fields are related by the useful Uzawa operator U_z defined as follows:

$$U_z\colon L_0^2(\Omega)\rightarrow L_0^2(\Omega),$$
$$P\rightarrow U_z(P),$$

such that $U_z(P)=\nabla\cdot\mathbf{v}(P)$, where $\mathbf{v}(P)$ satisfies

$$\alpha\mathbf{v}-\nu\nabla^2\mathbf{v}=-\nabla P. \tag{18}$$

The Uzawa operator is a self-adjoint isomorphism of $L_0^2(\Omega)$ and the associated bilinear form is symmetric and positive definite. These properties explain why pressure is commonly used to compute the unique divergence-free solution and, moreover, allow us to improve the previous gradient approach by the use of a conjugate gradient method. However, for simplicity we will always consider the pure gradient algorithm, the CG variant being just sketched and fully described in the Appendix. The Lagrangian formulation and proofs of convergence can be found in Fortin and Glowinski[24] (or in a less mathematical form in Cahouet and Hauguel[16]).

We must pay attention to this scheme because it satisfies most of the industrial requirements recalled in the Introduction:

(i) The extreme simplicity of the algorithm is obvious from the iterative process described above.
(ii) The robustness is related to the minimization process.
(iii) The mass conservation can be satisfied as precisely as necessary since the pressure belongs to $L^2(\Omega)$.
(iv) The same algorithm is able to deal with 2D or 3D modelling without any complication.
(v) Finally each iteration is rather cheap: only Step 1 requires a linear system solution and the matrix involved is sparse, rather well conditioned, of low-order (because each component can be computed independently) and can be factorized and preconditioned once and for all.

So this algorithm appears to be adequate, but unfortunately the speed of convergence is very slow, i.e. the L^2-norm of the residual divergence decays very slowly (see numerical results given later) and too many iterations are required to obtain sufficient accuracy.

Classical improvements

To cope with this major drawback, three interesting variants can be investigated: augmented Lagrangian, multigrid and preconditioning methods.

Considering the Uzawa scheme as a Lagrangian method (cf. Hestenes[25] and Powell[26]), Fortin and Glowinski[24] have suggested reinforcing the weight of the constraint in the functional $\mathscr{L}_1$ by adding the square of the L^2-norm of the divergence. They defined an augmented Lagrangian $\mathscr{L}_2$ as

$$\mathscr{L}_2(\mathbf{v}, P) = \mathscr{L}_1(\mathbf{v}, P) + (r/2)(\nabla \cdot \mathbf{v}, \nabla \cdot \mathbf{v}), \quad r \in \mathbb{R}_*^+. \tag{19}$$

Hence the Uzawa scheme is again available on the dual functional and leads to the same kind of iterative algorithm as the previous one, except that Step 1 has to be replaced by:

Step 1. Estimate the velocity from P^n by the modified equation

$$\alpha \mathbf{v}^n - \nu \nabla^2 \mathbf{v}^n + r \nabla(\nabla \cdot \mathbf{v}^n) = -\nabla P^n + \mathbf{s} \quad \text{on } \Omega, \tag{20}$$

with $\mathbf{v}^n = \mathbf{v}_\Gamma$ on Γ.

The greater r is the faster is the convergence, but the bigger is the condition number associated with the matrix of the linear system resulting from space discretization. Therefore the optimal value of r has to be found numerically. In most cases this algorithm is better than the previous Uzawa scheme and precise solutions are obtained in less than ten iterations. Meanwhile, the components of the velocity are now coupled by the addition of $r\nabla(\nabla \cdot \mathbf{v})$ and the size of the linear system is consequently increased (i.e. multiplied by two (resp. three) for 2D (resp. 3D) problems). So this elegant approach seems to be restricted to 2D problems.

The same limitation is relevant, at least up to now, to multigrid methods. Multiple variants have been considered by Verfurth[27,28] and Nigon[29] and very fast convergence rates (see numerical results) have been obtained on 2D regular meshes, but extensions to unstructured meshes and 3D problems are still under development.

In order to overcome these difficulties, we have been developing at EDF since 1981 a third complementary approach based on the use of preconditioners which will be discussed in the next section.

PRECONDITIONED UZAWA SCHEMES

Preconditioning method

Preconditioning appears naturally if the standard Uzawa algorithm is interpreted as an iterative solver for the equivalent pressure formulation:

$$\left.\begin{array}{l}\text{Find } P\in L_0^2(\Omega) \text{ such that}\\ U_z(P)=\nabla\cdot\mathbf{A}^{-1}\mathbf{f},\end{array}\right\}\tag{21}$$

i.e.

$$\left.\begin{array}{l}\text{Find } P \text{ such that}\\ \nabla\cdot\mathbf{A}^{-1}\nabla P=\nabla\cdot\mathbf{A}^{-1}\mathbf{f},\end{array}\right\}\tag{22}$$

with

$$\begin{gathered}\mathbf{A}^{-1}: H^{-1}(\Omega)^n\rightarrow H_0^1(\Omega)^n,\\ \mathbf{v}\rightarrow\mathbf{A}^{-1}(\mathbf{v}),\\ \mathbf{A}^{-1}(\mathbf{v})=(\alpha\mathbf{I}-\nu\nabla^2)^{-1}\mathbf{v},\\ \mathbf{v}=\mathbf{0}\quad\text{on}\,\Gamma.\end{gathered}\tag{23}$$

By definition, the computed solution $(P, \mathbf{v}(P))$ satisfies equations (1a) and (1b). The equivalence to the initial problem is derived from the Uzawa operator properties (as recalled in the previous section).

So it is natural to speed up the iterative process by introducing a symmetrical positive definite operator $\mathbf{C}$, close to U_z (in a sense to be defined), $\mathbf{C}$ being used as a preconditioner for the descent step as follows:

Step 3'. $$P^{n+1}=P^n-\rho\mathbf{C}^{-1}\nabla\cdot\mathbf{v}^n.\tag{17'}$$

As only Step 3 has been modified, all the good properties of the method (and especially the uncoupling of velocity components) are preserved, provided that the computation of $\mathbf{C}^{-1}$ is not too expensive.

As will be clearly demonstrated by the numerical results, the rate of convergence of the preconditioned scheme is very sensitive to the choice of $\mathbf{C}$. At least five categories of method allow us to build different variants for $\mathbf{C}$.

(i) The most classical approach is based on an algebraic approximation of the matrix associated with the discretized formulation, as for example incomplete Choleski decomposition. Unfortunately none of these methods[29] can be applied to the Uzawa operator, which is never built in practice in order to save CPU time and reduce memory requirements.

(ii) In a second more heuristic approach, the initial operator is degenerated depending on the flow characteristics. In the case of high Reynolds number a method introduced by Labadie and Lasbleiz[31] will be detailed hereafter.

(iii) This approach can be generalized by introducing the Fourier analysis of the Uzawa operator. Thus we can study the behaviour of different variants and propose a preconditioner C, close to U_z in a spectral meaning.[16]

(iv) This kind of preconditioner can also be deduced from a multi-solver approach[32] similar to the multigrid method, which allows an understanding of the quality of the numerical results.

(v) Finally the last approach, which is still under development,[5,33] is based on a quasi-Newton method and takes into account the updating and optimization of previous preconditioners with time evolution.

Labadie's approach

Let us consider first the approach developed by Labadie. For high Reynolds number it seems natural to neglect the viscous terms in the core of the flow; this is equivalent to assimilating the velocity contribution in equation (1b) in the unsteady part:

$$\mathbf{A}=\alpha\mathbf{I}-\nu\boldsymbol{\nabla}^2\sim\alpha\mathbf{I}. \tag{24}$$

Then the Uzawa operator is simplified as

$$U_z(P)\sim\boldsymbol{\nabla}(\alpha\mathbf{I})^{-1}\boldsymbol{\nabla}P\sim(1/\alpha)\boldsymbol{\nabla}^2P. \tag{25}$$

The lack of boundary conditions can be overcome by assuming the existence of a boundary layer which allows us to use

$$\partial P/\partial n=0 \tag{26}$$

near the solid walls. So a first preconditioner $\mathbf{C}_1$ is fully defined by its inverse $\mathbf{C}_1^{-1}$:

$$\begin{aligned}\mathbf{C}_1^{-1}\colon L_0^2(\Omega)&\to H^1(\Omega),\\ q&\to P=\mathbf{C}_1^{-1}(q),\end{aligned}$$

such that

$$\begin{aligned}&-\boldsymbol{\nabla}^2P=q \quad \text{on } \Omega,\\ &\partial P/\partial n=0 \quad \text{on } \Gamma, \qquad \int_\Omega P\,\mathrm{d}\Omega=0.\end{aligned} \tag{27}$$

Step 3 of the Uzawa algorithm becomes formally

$$P^{n+1}=P^n-\rho(-\boldsymbol{\nabla}^2)^{-1}(\boldsymbol{\nabla}\cdot\mathbf{v}^n). \tag{17''}$$

This preconditioner is especially attractive, because it satisfies all the mathematical properties required (correct functional spaces, same kernel as the U_z operator, symmetrical positive definite properties of the associated bilinear form) and furthermore the first iteration includes the classical Chorin–Temam[12,13] scheme, which obviously provides a good predictor to start the iterative process.

For numerical applications the C_1 operator, defined only on pressure unknowns, is discretized and factorized once and for all. It appears from numerical experiments that this preconditioner coupled with the conjugate gradient variant considerably increases the efficiency of the Uzawa scheme at a very reasonable cost. More precisely, the performances are related to the mesh Reynolds number

$$Re_{\mathrm{M}}=\frac{\alpha \mathrm{D}X^2}{\nu}\quad\left(=Re\frac{(\mathrm{D}X/\mathrm{D}T)}{U}\frac{\mathrm{D}X}{L}\quad \text{if } \alpha=\frac{1}{\mathrm{D}T}\right), \tag{28}$$

which takes into account the influence of the time step and the mesh refinement characterized by a reference length DX. The bigger Re_{M} is (i.e. the smaller the time step or the coarser the grid), the faster is the algorithm.

On the other hand, the above approach has some drawbacks:

(i) The boundary conditions on P^n remain unchanged during iterations, since we have

$$\frac{\partial P^n}{\partial n}=\frac{\partial P^{n-1}}{\partial n}=\ldots=\frac{\partial P^0}{\partial n}\quad \text{on } \Gamma, \tag{29}$$

which can clearly be inaccurate if the first guess P^0 is wrong.

(ii) The scheme generally behaves poorly at low Reynolds mesh numbers, which corroborates the underlying assumptions.

(iii) This approach assumes implicitly that P belongs to $H^1(\Omega)$. From this point of view the preconditioner acts as a smoother for the residual divergence, which is only supposed to belong to $H^{-1}(\Omega)$ because of duality, and thus can be used even for $Re_{\mathrm{M}}=0$ if all the given data are sufficiently smooth (see Theorem 2), as for the steady Couette flow for example.

These limitations on pressure regularity and mesh Reynolds number have motivated us to pursue our studies of preconditioning.

Present approach

Fourier analysis. In order to provide a quantitative analysis of the behaviour of the solvers with respect to the regularity of pressure, we have achieved a spectral comparison of each solver described herein. To avoid a complete recall of the Fourier analysis formalism (see Lions and Magenes[34] for details), we only give a simplified calculation based on the basic Uzawa formulation and then sum up equivalent results for the other solvers.

Let us consider the nth iteration of a Uzawa scheme applied to a periodic boundary GSP and assume that the residual divergence is equal to

$$\nabla\cdot\mathbf{v}^n=\mathrm{e}^{-\mathrm{i}\boldsymbol{\omega}\cdot\mathbf{x}},\quad (\boldsymbol{\omega},\mathbf{x})\in\mathbb{R}^n\times\mathbb{R}^n,\quad \mathrm{i}^2=-1 \tag{30}$$

(the complete spectrum being obtained by superposition owing to the linearity of the operators). Then we easily deduce the pressure and velocity increments, varying with respect to the value of the descent parameter ρ as

$$\delta P^n=-\rho\nabla\cdot\mathbf{v}^n=-\rho\mathrm{e}^{-\mathrm{i}\boldsymbol{\omega}\cdot\mathbf{x}}. \tag{31}$$

then $\delta\mathbf{v}^n$ fulfilling

$$\alpha\delta\mathbf{v}^n-\nu\nabla^2\delta\mathbf{v}^n=-\nabla\delta P^n=-\mathrm{i}\rho\boldsymbol{\omega}\mathrm{e}^{-\mathrm{i}\boldsymbol{\omega}\cdot\mathbf{x}} \tag{32}$$

is easily reckoned as

$$\delta\mathbf{v}^n=-\rho\frac{\mathrm{i}\boldsymbol{\omega}}{\alpha+\nu\|\boldsymbol{\omega}\|^2}\mathrm{e}^{-\mathrm{i}\boldsymbol{\omega}\cdot\mathbf{x}}, \tag{33}$$

$$\nabla\cdot\delta\mathbf{v}^n=\frac{-\rho\|\boldsymbol{\omega}\|^2}{\alpha+\nu\|\boldsymbol{\omega}\|^2}\mathrm{e}^{-\mathrm{i}\boldsymbol{\omega}\cdot\mathbf{x}}. \tag{34}$$

So the residual divergence becomes after a single Uzawa iteration

$$\nabla\cdot\mathbf{v}^{n+1}=\nabla\cdot\mathbf{v}^{n}+\nabla\cdot\delta\mathbf{v}^{n}=\left(1-\frac{\rho\|\boldsymbol{\omega}\|^{2}}{\alpha+\nu\|\boldsymbol{\omega}\|^{2}}\right)\mathrm{e}^{-\mathrm{i}\boldsymbol{\omega}\cdot\mathbf{x}}. \tag{35}$$

The iterative process converges if

$$\left|1-\frac{\rho\|\boldsymbol{\omega}\|^{2}}{\alpha+\nu\|\boldsymbol{\omega}\|^{2}}\right|\leqslant 1\Leftrightarrow 0\leqslant\rho\leqslant\frac{2(\alpha+\nu\|\boldsymbol{\omega}\|^{2})}{\|\boldsymbol{\omega}\|^{2}} \tag{36}$$

and the optimal value for ρ is obviously

$$\rho_{\mathrm{opt}}^{\mathrm{Uz}}=\nu+\alpha/\|\boldsymbol{\omega}\|^{2}. \tag{37}$$

Thus it appears that the optimal value is strongly related to the shape (i.e. the spectral decomposition) of the pressure field. The same analysis applied to the Labadie solver leads to

$$\rho_{\mathrm{opt}}^{\mathrm{Lab}}=\alpha+\nu\|\boldsymbol{\omega}\|^{2}. \tag{38}$$

In the same manner the dependence of the optimal descent parameter with respect to ω for the augmented Lagrangian method is given by

$$\rho_{\mathrm{opt}}^{\mathrm{AL}}=\nu+r+\alpha/\|\boldsymbol{\omega}\|^{2}. \tag{39}$$

These dependencies are summed up in Figure 3. From these curves we can estimate the sensibility of ρ_{opt} with respect to the frequency. These graphs prove that the classical Uzawa

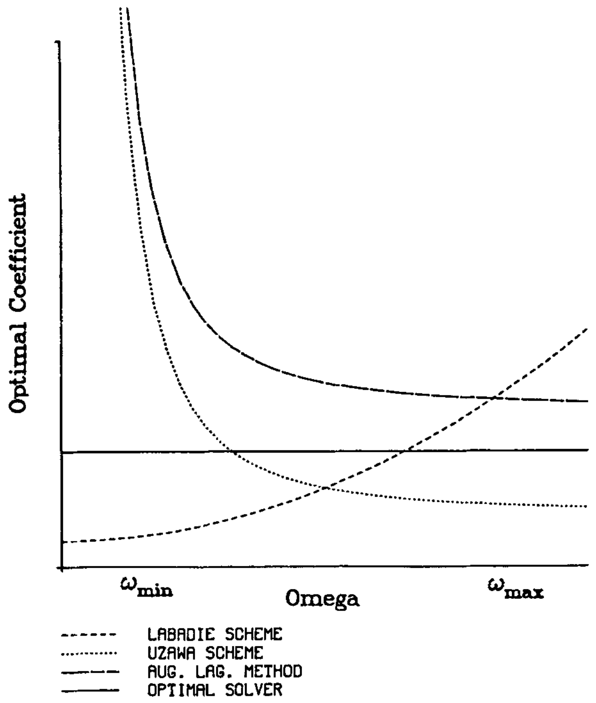

Figure 3. Comparison of different schemes

scheme is able to filter all the high frequencies ($\|\boldsymbol{\omega}\| \gg \alpha/\nu$) in a single iteration if ρ is chosen equal to ν, but the convergence for low frequencies will be very slow (if the spectrum is not monochromatic!) because the value of ρ will not be optimal and the spectral radius will be close to one. On the other hand, the Labadie scheme behaves well for long waves (with $\rho = \alpha$) but is not able to capture short wiggles, and this is in perfect agreement with numerical tests. Finally the analysis of the augmented Lagrangian curve clearly exhibits that the penalization of the constraint (in an L^2-norm) allows us to translate the spectrum proportionally to r and thus increases the efficiency of the basic scheme for the short waves. Moreover, equation (39) justifies the empirical choice $\rho = r$ introduced by Fortin and Glowinski.[24]

To conclude this comparison, let us notice that in practical cases $\|\boldsymbol{\omega}\|$ is bounded by $\omega_{\min}$ and $\omega_{\max}$, taking into account the smallest finite element diameter and the size of the domain. As the initial Fourier transform of divergence covers all this bandwidth, the choice of ρ is strongly related to the minimization process (i.e. to the choice of the scalar product), but most of them favour long waves. So the Uzawa scheme is more handicapped than the Labadie scheme, which is able to suppress long-wave components during the first iterations and seems more powerful, at least at the beginning.

These analytical results lead us to consider a new class of preconditioners defined as a linear combination of the identity operator (from the Uzawa scheme) and the inverse of the delta operator (from the Labadie approach):

$$\mathbf{C}_2^{-1} = \lambda \mathbf{I}^{-1} - \mu(\boldsymbol{\nabla}^2)^{-1}, \quad (\lambda, \mu) \in \mathbb{R} \times \mathbb{R}. \tag{40}$$

The required property of $\mathbf{C}_2^{-1}$ as a preconditioner (i.e. to be a self-adjoint isomorphism onto $L_0^2(\Omega)$) implies obviously

$$(\lambda, \mu) \in \mathbb{R}_*^+ \times \mathbb{R}^+. \tag{41}$$

Then our simplified Fourier analysis provides the optimal descent parameter with respect to the frequency as

$$\rho_{\text{opt}}^{\mathrm{C}} = \frac{\alpha + \nu \|\boldsymbol{\omega}\|^2}{\mu + \lambda \|\boldsymbol{\omega}\|^2} \tag{42}$$

and an optimal choice for the GSP appears to be

$$\lambda = \nu, \qquad \mu = \alpha, \tag{43}$$

because the descent parameter becomes fully independent of the frequency and the scheme is able to span all the spectrum with the same efficiency as a multigrid scheme. Mathematically this choice ensures the equality of the symbols of the U_z and $\mathbf{C}_2$ operators, at least in the case of periodic boundary conditions, which appear for example in turbomachinery studies. Moreover, one could consider optimizing the (λ, μ) parameters for other kinds of boundary conditions, but the numerical results show that this estimation is sufficiently precise for Dirichlet BCs (in any case these values are still optimal far from the boundary).

This new preconditioner, whose inverse is defined as

$$\mathbf{C}_2^{-1} = \nu \mathbf{I}^{-1} - \alpha(\boldsymbol{\nabla}^2)^{-1}, \tag{44}$$

includes Labadie's ideas for strongly unsteady configurations and degenerates in a simple manner for steady or quasi-steady cases ($\alpha \sim 0$). For intermediate situations it specifies the optimal ratio between the two components. Before detailing some numerical experiments, let us justify and explain these improvements by a complementary analysis based on a multi-solver approach.

Multi-solver approach. The main idea underlying this section is that the efficiency of solvers is strongly related to pressure regularity. More precisely, while Chorin–Temam,[12,13] Glowinski–Pironneau[35] and Labadie[31] methods are well suited for regular and smooth solutions, only the (CG) Uzawa algorithm (which does not require $P \in H^1(\Omega)$) is able to solve stiff problems.

This numerical intuition leads us to develop concurrently a multi-solver approach coupling the Uzawa scheme with a smooth solver; the first one being dedicated to compute sharp gradients and the second one to obtain quickly the smooth part of the field which represents 90% of the whole domain in most of the cases. Initially our idea was to transpose the multigrid concept (see Hackbusch[36] for basis) to a multi-operator concept as follows:

$$\text{Refined grid} \Leftrightarrow L^2(\Omega) \Leftrightarrow \text{Uzawa scheme,}$$

$$\text{Coarse grid} \Leftrightarrow H^1(\Omega) \Leftrightarrow \begin{cases} \text{Chorin–Temam scheme,} \\ \text{Glowinski–Pironneau scheme,} \\ \text{Labadie scheme.} \end{cases}$$

We hope to reach in this way the efficiency of the multigrid approach (i.e. a rate of convergence independent of the spectral decomposition of P^{28}) without generating embedded grids, something that has not been feasible up to now for complicated 3D domains.

For the sake of simplicity we first consider the simplest pair, Uzawa–Chorin. If we denote by $(P^n, \mathbf{v}^n)$ the solution obtained at iteration n from a CG Uzawa algorithm, the deviation $(\delta P^n, \delta \mathbf{v}^n)$ from the exact solution is given by

$$\begin{aligned} \alpha\delta\mathbf{v}^n - \nu\nabla\cdot\delta\mathbf{v}^n &= -\nabla\delta P^n \quad \text{over } \Omega, \\ \nabla\cdot\delta\mathbf{v}^n &= -\nabla\cdot\mathbf{v}^n \quad \text{over } \Omega, \\ \delta\mathbf{v}^n &= 0 \quad \text{on } \Gamma. \end{aligned} \tag{45}$$

Then formally

$$-\nabla^2\delta P^n = \alpha\nabla\cdot\delta\mathbf{v}^n - \nu\nabla^2(\nabla\cdot\delta\mathbf{v}^n) \tag{46}$$

$$= -\alpha\nabla\cdot\mathbf{v}^n + \nu\nabla^2(\nabla\cdot\mathbf{v}^n). \tag{47}$$

As for the Chorin–Temam approach, Neumann homogeneous boundary conditions are chosen for the Laplacian operator. Hence the iterative process on pressure becomes

$$P^{n+1} = P^n - \rho(\alpha\mathbf{I}^{-1} - \nu(\nabla^2)^{-1})\nabla\cdot\mathbf{v}^n \tag{48}$$

and we recognize the previous preconditioner $\mathbf{C}_2$ obtained initially by the Fourier analysis. As before, the main approximation is related to the boundary conditions. However, this multi-solver approach introduces a new point of view which allows us to conceive an improvement for $\mathbf{C}_2$, not in the choice of (λ, μ) but rather in the choice of the boundary conditions. This can easily be done by replacing the crude Chorin–Temam scheme by a few iterations of a Glowinski–Pironneau solver as the smoother.

The next section is devoted to the discretization and validation of these methods on 2D and 3D numerical experiments.

DISCRETE CASE AND NUMERICAL RESULTS

Discrete formulation of the GSP

We discretize the weak formulation of the GSP by choosing two subsets V_h and M_h approximating $H_0^1(\Omega)$ and $L^2(\Omega)$. Then the discrete form is the following:

$$\left.\begin{array}{l}\text{Find } (\mathbf{v}, P)\in V_h\times M_h \text{ such that}\\ a(\mathbf{v}, \varphi)-(P, \nabla\cdot\varphi)=(\mathbf{f}, \varphi) \quad \forall\varphi\in V_h, \\ (\pi, \nabla\cdot\mathbf{v})=0 \quad \forall\pi\in M_h,\end{array}\right\} \qquad \begin{array}{r}\\(49\text{a})\\(49\text{b})\end{array}$$

where (. , .) is the L^2-inner product and $a(. , .)$ the bilinear form defined by

$$a(\varphi, \psi)=\int_\Omega (\alpha\varphi\cdot\psi+\nu\nabla\varphi\cdot\nabla\psi)\mathrm{d}\Omega \quad \forall(\varphi, \psi)\in V_h\times V_h. \tag{50}$$

Taking into account the boundary conditions, the matrix form of the weak formulation can be written as

$$\begin{bmatrix}\mathbf{A}\,\mathbf{B}^{\mathrm{T}}\\ \mathbf{B}\,\mathbf{0}\end{bmatrix}\begin{bmatrix}\mathbf{U}\\ \mathbf{P}\end{bmatrix}=\begin{bmatrix}\mathbf{F}\\ \mathbf{0}\end{bmatrix}, \tag{51}$$

where **U** and **P** denote the vectors of nodal velocity and nodal pressure values respectively and where **A** and **B** are the matrix blocks

$$\mathbf{A}=(a_{i,j}) \quad \text{with} \quad a_{i,j}=a(\varphi_i, \boldsymbol{\varphi}_i), \tag{52}$$

$$\mathbf{B}=(b_{i,j}) \quad \text{with} \quad b_{i,j}=-(\pi_i, \nabla^{\mathrm{T}}\varphi_i). \tag{53}$$

Of course the finite element approximations of **v** and P have to satisfy some compatibility condition in order to ensure the existence and unicity of the solution $(\mathbf{U}, \mathbf{P})^{\mathrm{T}}$ of the linear system (51).

For all the following numerical results we have chosen the Hood–Taylor[37] approach, i.e. P_1–P_2 six-node triangles for 2D or ten-node tetrahedra for 3D, with continuous pressure, for which the space approximation is second-order accurate. Note that any other choice of finite elements, such as Q_1–Q_2 quadrilaterals, or bricks, or P_1–isoP_1 triangles[6] or tetrahedra, is also compatible with our approach.

Discrete Uzawa algorithm

The discretized Uzawa pressure formulation derived from the elimination of the velocity in equation (49a) using equation (49b) (cf. equation (21)) appears to be equivalent to the linear system on pressure nodal values,

$$[\mathbf{B}\mathbf{A}^{-1}\mathbf{B}^{\mathrm{T}}]\,[\mathbf{P}]=[\mathbf{B}\mathbf{A}^{-1}\mathbf{F}], \tag{54}$$

which is solved iteratively as follows:

Step 0. Initialize $\mathbf{P}_n$.

Step 1. estimate the velocity, component by component, by solving

$$\mathbf{A}\mathbf{U}_n=-\mathbf{B}^{\mathrm{T}}\mathbf{P}_n+\mathbf{F}. \tag{55}$$

Step 2. Estimate the residual of the pressure system, which is in fact the divergence of $\mathbf{U}_n$:

$$\mathbf{R}_n = \mathbf{B}\mathbf{A}^{-1}\mathbf{F} - \mathbf{B}\mathbf{A}^{-1}\mathbf{B}^{\mathrm{T}}\mathbf{P}_n = \mathbf{B}\mathbf{U}_n. \tag{56}$$

Step 3. Compute the new descent direction

$$\mathbf{P}_{n+1} = \mathbf{P}_n - \rho\mathbf{R}_n. \tag{57}$$

By analogy with the continuous case, a good discretization of the preconditioner **C** has to be close to the discretized Uzawa operator in the following sense:

$$\mathbf{C}^{-1}[\mathbf{B}\mathbf{A}^{-1}\mathbf{B}^{\mathrm{T}}] \sim \mathbf{I}. \tag{58}$$

Then if we assume, as Labadie did, that the Reynolds number is very high, the inertial term predominates over the viscous term in the matrix **A** and we have

$$\mathbf{A} \sim \alpha\mathbf{M}_{\mathrm{V}}^{-1}, \tag{59}$$

where $\mathbf{M}_{\mathrm{V}}$ denotes the P_2 mass matrix.

Hence we obtain a discrete approximation of **C** as

$$\mathbf{C}_1 = \mathbf{B}\mathbf{M}_{\mathrm{V}}^{-1}\mathbf{B}^{\mathrm{T}}, \tag{60}$$

which is nothing but the so-called compatible Laplacian discretization often advocated by finite difference users.[38] Let us notice that a direct discretization of **C** leads to the classical Laplacian discretization with homogeneous Neumann boundary conditions:

$$\mathbf{D} = (d_{i,j}) \quad \text{with} \quad d_{i,j} = -(\nabla\pi_i, \nabla\pi_j). \tag{61}$$

Both discretizations of the pressure Laplacian will be used and compared hereafter. Let us point out that the same choice arises for our new preconditioner, which involves moreover the P_1 pressure mass matrix $\mathbf{M}_{\mathrm{P}}$.

Numerical results

Convergence rate. In order to compare in an objective way the performances of the different schemes presented in the previous section, we have chosen (according to Verfurth[28]) to describe the decay of the L^2-norm of the divergence versus the number of iterations. All these curves can be characterized by the rate of convergence χ, defined as

$$\chi = \left(\frac{\|\nabla\cdot\mathbf{v}_n\|}{\|\nabla\cdot\mathbf{v}_0\|}\right)^{1/n} \sim \left(\frac{\|\mathbf{B}\mathbf{U}_n\|}{\|\mathbf{B}\mathbf{U}_0\|}\right)^{1/n}, \tag{62}$$

which is strongly related to the condition number $\mathscr{C}$ of the matrix $\mathbf{C}^{-1}\mathbf{B}\mathbf{A}^{-1}\mathbf{B}^{\mathrm{T}}$, as shown in the classical upper-bound estimation[30]

$$\chi \leqslant \frac{\sqrt{\mathscr{C}}-1}{\sqrt{\mathscr{C}}+1} \tag{63}$$

derived for the conjugate gradient approach. In semi-logarithmic axes as shown in Figures 4–7, χ is equal to the inverse of the logarithm of the slope: the lower χ is, the better is the scheme. However, comparisons must be done carefully because χ depends in most cases on the regularity of the pressure field and on the mesh Reynolds number defined earlier.

2D comparative analysis of preconditioners. For the following 2D results, P_2–P_1 finite elements and classical discretization **D** of the Laplacian have been used. The next four numerical tests are intended to compare the performances and the sensitivity of the different schemes with respect to the pressure regularity, the mesh Reynolds number and the mesh refinement. When possible, χ estimates are compared with Verfurth's[28] multigrid results.

A smooth test. The first numerical test deals with a smooth analytical solution which belongs to the space $V_h \times M_h$. It considers a 2D unit square domain with homogeneous boundary conditions on velocity and a constant volume force $\mathbf{f}=(-1, 1)$. Thus the exact solution is

$$\mathbf{v}=\mathbf{0}, \qquad P=-x+y+\text{constant}. \tag{64}$$

The following results are obtained with $DX=1/10$, where DX denotes the smallest distance between two pressure nodes. The rate of convergence of the various schemes is presented in Table I. Let us emphasize that χ has to be less than one in order for the scheme to converge and a value for χ of about 0·3 means that the residual divergence is divided by ten every two iterations. Then one can appreciate the speed-up resulting from preconditioning techniques which appear to be even more powerful than multigrid schemes in that case.

Influence of singularities. After this very smooth test, we can consider a less regular computation including a slit in the domain and a stiff boundary condition on the velocity. Numerical results are summarized on Table II; they compare the evolution of divergence for the different schemes in the steady and unsteady cases.

In both cases the new approach is still better, with an excellent convergence rate. In fact for all our 2D tests the value of χ obtained with the present scheme is quite constant ($0{\cdot}20 \leqslant \chi \leqslant 0{\cdot}31$ for

Table I. Comparison of the rate of convergence for the smooth test

Case	Classical Uzawa scheme	Labadie approach	Present approach	Verfurth multigrid
Steady ($Re_M=0$)	$0{\cdot}6\leqslant\chi\leqslant 1$	$0{\cdot}4\leqslant\chi\leqslant 0{\cdot}8$	0·34	$0{\cdot}5\leqslant\chi\leqslant 0{\cdot}9$
Unsteady ($Re_M=10$)	1	$0{\cdot}4\leqslant\chi\leqslant 0{\cdot}6$	0·28	—

Table II. Comparison of the convergence rate test of the cavity with a slit

Case	Classical Uzawa scheme	Labadie approach	Present approach
Steady ($Re_M=0$)	$\chi\leqslant 0{\cdot}7$	0·56	0·46
Unsteady ($Re_M=10$)	$\chi\leqslant 0{\cdot}8$	0·46	0·31

unsteady cases, $0{\cdot}25 \leqslant \chi \leqslant 0{\cdot}46$ for steady cases) and of the same order of magnitude as with multigrid methods.

Influence of the mesh Reynolds number. To study the simultaneous influence of time and space discretization through the mesh Reynolds number, the classical lid driven cavity test has been chosen with 'smooth' boundary conditions (i.e. $\mathbf{v}=(x^2-x, 0)$ on the moving wall).

The mesh Reynolds number takes the following values: 0, 0·1, 10 and 100 with (DX fixed at 1/10). The decay of the divergence has been drawn in Figure 4 and it confirms that:

(i) Labadie's approach is well suited for strongly unsteady cases ($\chi \sim 0{\cdot}35$) but has a poor rate of convergence when $Re_{\mathrm{M}} \geqslant 50$ ($\chi \geqslant 0{\cdot}8$).
(ii) Our new scheme is independent of Re_{M} and leads to a very good solver ($\chi = 0{\cdot}3$) even on this difficult test problem where the continuous solution does not belong to $L^2(\Omega)$.

Influence of the mesh size. It is well known that the efficiency of most of the solvers is reduced when the mesh is refined (because of the deterioration of the condition number associated with the matrix of the system to be solved), except for multigrid schemes, which are able to deal with high frequencies.[28,36] Taking into account analogies between the multigrid and multi-solver approaches described earlier, we presume that our new scheme has the same properties.

Thus we have performed a study of the influence of the mesh size on the test case of flow behind a circular cylinder[39] by using successive mesh refinements (Table III).

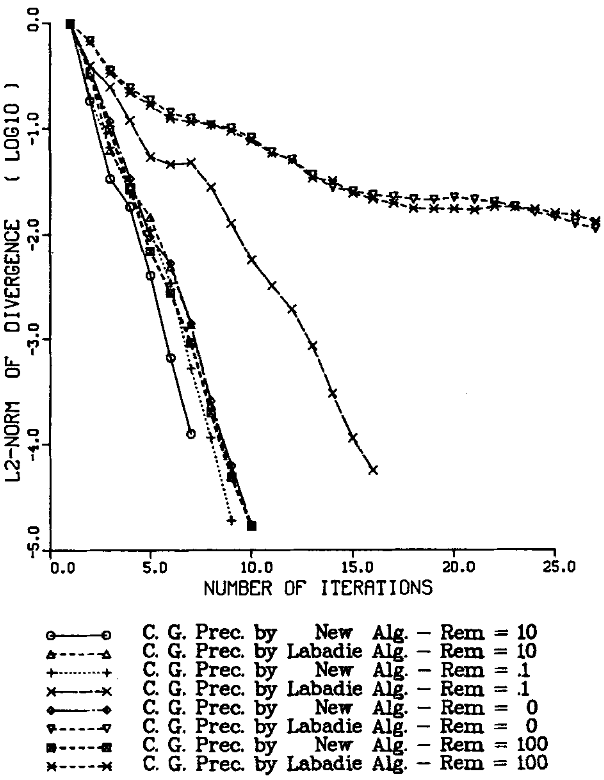

Figure 4. Influence of the Reynolds mesh number

Table III. Description of the meshes used

Mesh	Number of elements	Number of velocity nodes	Number of pressure nodes
Coarse	470	1020	275
Reference	1128	2380	626
Intermediate	1458	3028	784
Refined	3168	6502	1666

Two parameters are varying here: the mesh Reynolds number and the total number of nodes. The results presented in Figure 5 confirm that our new preconditioner is not affected (χ is still about 0·30), while the Laplacian efficiency decreases as Re_M decreases.

Comparison of the discretizations of the pressure Laplacian. As explained before, another discretization of the Laplacian, involving **B** and $\mathbf{M}_V^{-1}$, is available; it seems more fruitful because

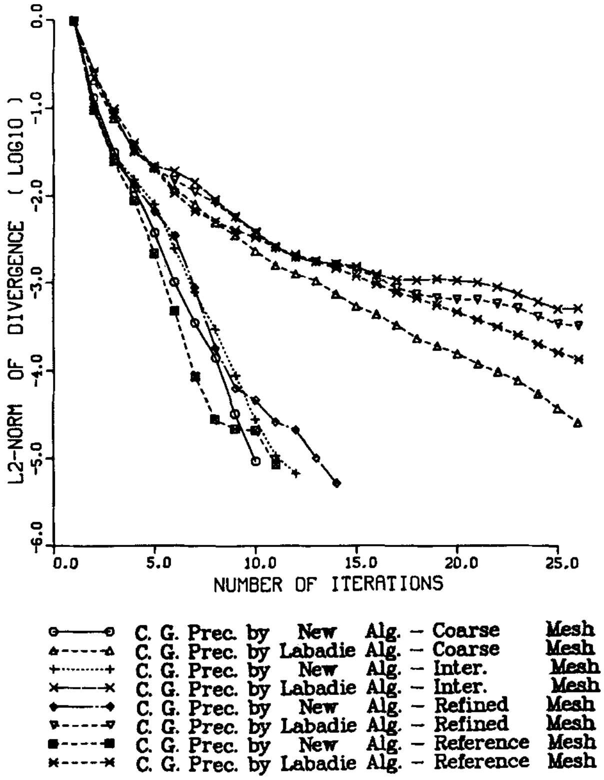

Figure 5. Influence of space discretization; cylinder test

it takes into account the velocity approximation and includes the exact pressure boundary conditions. But it requires the computation of the inverse of $\mathbf{M}_V$, which is a full matrix which cannot be stored for an industrial 3D case. Nevertheless it is still possible for small 2D problems, and comparisons have been done.

As an example, Figure 6 compares these two variants of Labadie's preconditioner, for various Reynolds mesh numbers (ranging from 0 to 100), for the lid driven cavity test. As expected, the compatible approximation is better, and especially when Re_M vanishes. For 3D problems research is still under way for a good approximation of $\mathbf{M}_V^{-1}$. Some preliminary results have been obtained using the inverse of the diagonal coefficients as the lumped P_2 mass matrix is not invertible.

3D comparative analysis of preconditioners with respect to the mesh refinement. All the 3D results presented have been obtained with P_2–P_1 ten-node tetrahedra with continuous pressure. As explained above, we have combined inside our new preconditioner the pressure mass matrix and either the classical discretization **D** of the Laplacian or the matrix **B** (diag $\mathbf{M}_V)^{-1}\mathbf{B}^T$.

As for the 2D case, a study of the sensitivity of the solvers with respect to the size of the mesh has been performed for the 3D lid driven cavity test with a constant velocity imposed on the upper wall, i.e. including some pressure singularities near the corners. Three regular meshes have been built, dividing by two and three the size of the initial mesh on each boundary (Table IV).

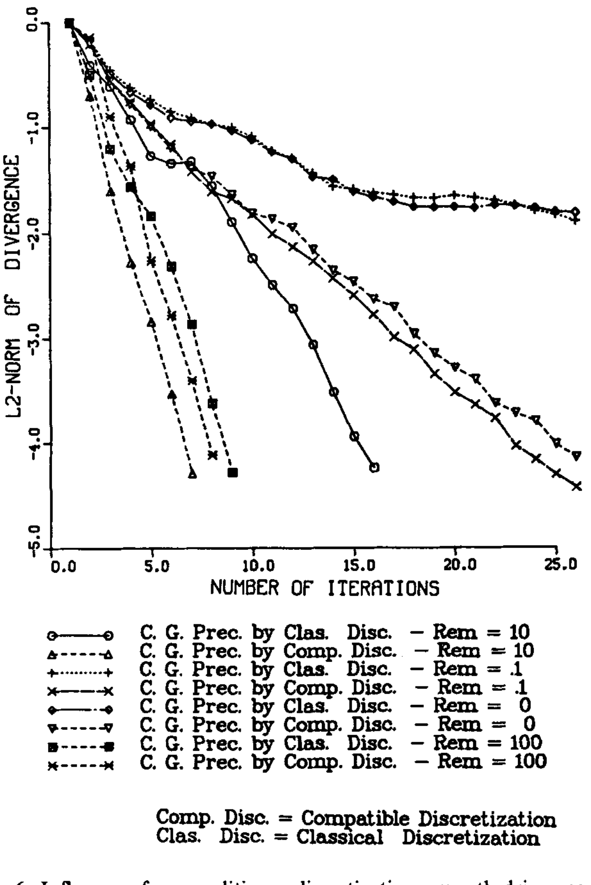

Figure 6. Influence of preconditioner discretization; smooth driven cavity test

Table IV. Mesh characteristics

Mesh	Number of elements	Number of velocity nodes	Number of pressure nodes	Percentage of constrained nodes	Number of degrees of freedom
Coarse 11 × 11 × 11	750	1331	216	45%	2412
Intermediate 21 × 21 × 21	6000	9261	1331	26%	21890
Refined 31 × 31 × 31	20250	29791	4096	18%	77382

Table V. Convergence rates for the 3D unsteady lid driven cavity (clas. disc., classical discretization of the Laplacian; comp. disc., approximation of the compatible discretization)

Mesh	Without prec.	Labadie prec. clas. disc.	Labadie prec. comp. disc.	Present prec. clas. disc.	Present prec. comp. disc.
Coarse	$0\cdot67\leqslant\chi\leqslant0\cdot95$	$0\cdot47\leqslant\chi\leqslant0\cdot75$	0·14	$0\cdot3\leqslant\chi\leqslant0\cdot49$	0·14
Intermediate	$0\cdot77\leqslant\chi\leqslant1$	$0\cdot54\leqslant\chi\leqslant0\cdot71$	0·15	$0\cdot3\leqslant\chi\leqslant0\cdot5$	0·15
Refined	0·98	$0\cdot52\leqslant\chi\leqslant0\cdot71$	0·14	$0\cdot3\leqslant\chi\leqslant0\cdot5$	0·14

Table VI. Convergence rates for the 3D steady lid driven cavity

Mesh	Without prec.	Labadie prec. clasc. disc.	Labadie prec. comp. disc.	Present prec.
Coarse	$0\cdot82\leqslant\chi\leqslant1$	$0\cdot82\leqslant\chi\leqslant1$	0·50	0·58
Intermediate	$0\cdot89\leqslant\chi\leqslant0\cdot94$	0·89	0·70	0·56
Refined	$0\cdot86\leqslant\chi\leqslant1$	0·92	0·78	0·57

On each mesh, two mesh Reynolds numbers have been compared: a value of 0 for the steady problem and a value of 10 for the unsteady flow. These parameters have been chosen because they characterize the most delicate situations, the differences in efficiency vanishing when the mesh Reynolds number is greater than 100. For these computations an example of the divergence decay is given in Figure 7 and convergence rates are described in Tables V and VI.

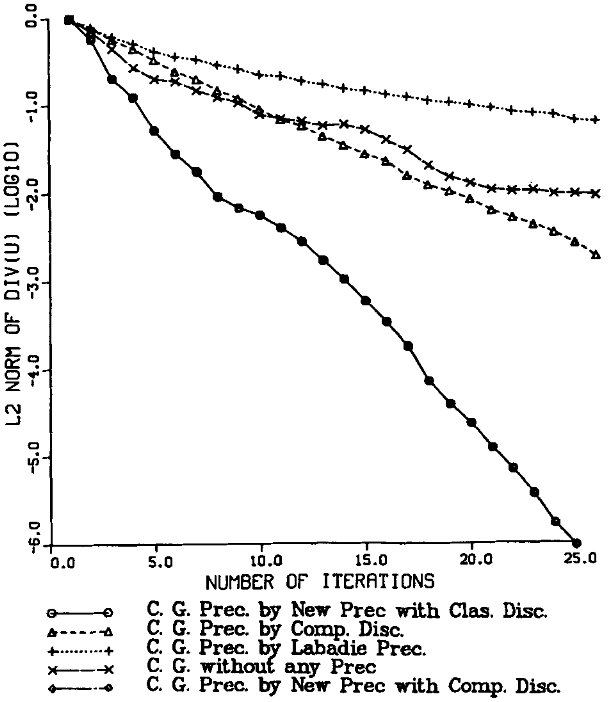

Figure 7(a). Steady 3D lid driven cavity (31 x 31 x 31)

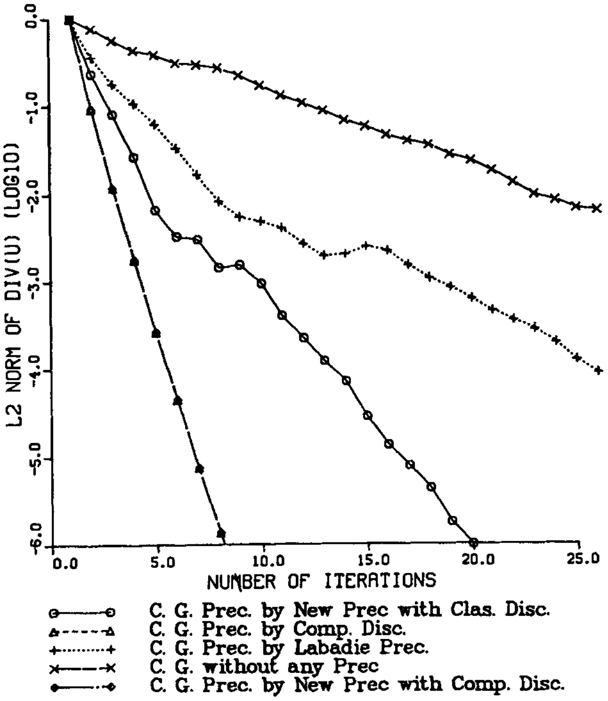

Figure 7(b). Unsteady 3D lid driven cavity (31 x 31 x 31)

A detailed analysis of the different curves and tables suggests the following remarks:

(i) In all cases the basic Uzawa scheme is prohibited.
(ii) For the unsteady equations the shape of the different curves is independent of DX, which clearly demonstrates that Re_{M} is an intrinsic parameter.
(iii) As expected for the steady case, the use of the Laplacian operator is not adapted and the rate of convergence increases quickly as the mesh is refined; nevertheless, the compatible approximation is always better, especially when the percentage of constrained nodes is significant.
(iv) On the other hand, although it is not always more efficient, the new preconditioner with the classical discretization of the Laplacian is more reliable, with a constant rate of convergence of about 0·5 for any mesh Reynolds number.

CPU time comparison for the 3D *lid driven cavity test.* An objective comparison of the various solvers must take into account the respective CPU costs, the memory requirements being identical. In Tables VII and VIII we summarize the CPU time required for an iteration in each solver in the steady and unsteady cases; these results have been obtained using a CRAY XMP 216 computer without multitasking.

Taking into account the convergence rate associated with each algorithm, these tables clearly show that for a given accuracy:

(i) Labadie's preconditioner and the new one (with compatible discretization of the Laplacian) are the cheapest in the unsteady configuration.
(ii) When the Reynolds number is decreasing, our new scheme with a classical discretization has to be preferred.
(iii) In the steady configuration these results have to be moderated by a complementary analysis of the matrix assembly cost, which prohibits the use of the compatible discretization.

An industrial application. For EDF purposes we have to deal with complicated geometries such as the cold plenum of a liquid metal fast breeder reactor (LMFBR) described in Figure 1. A refined finite element mesh of this domain has required about 20 000 velocity nodes (i.e. about 10^5 degrees of freedom for a turbulent simulation using a k–ε model). Figure 8 illustrates the decay of the divergence for the various schemes; it validates the previous analysis (the value of χ is indeed about 0·5) and confirms the adequacy of our solvers for this kind of problem.

Table VII. Unsteady computation: CPU time in seconds for one iteration

Mesh	Without prec.	Labadie prec. clas. disc.	Labadie prec. comp. disc.	Present prec. clas. disc.	Present prec. comp. disc.
Coarse	0·075	0·08	0·1	0·085	0·11
Intermediate	0·7	0·77	1·05	0·9	1·15
Refined	2·5	2·8	4·0	3·5	4·5

Table VIII. Steady computation: CPU time in seconds for one iteration

Mesh	Without prec.	Labadie prec. clasc. disc.	Labadie prec. comp. disc.	Present prec.
Coarse	0·13	0·14	0·15	0·135
Intermediate	2·1	2·6	2·5	2·2
Refined	9	13·5	13	9·5

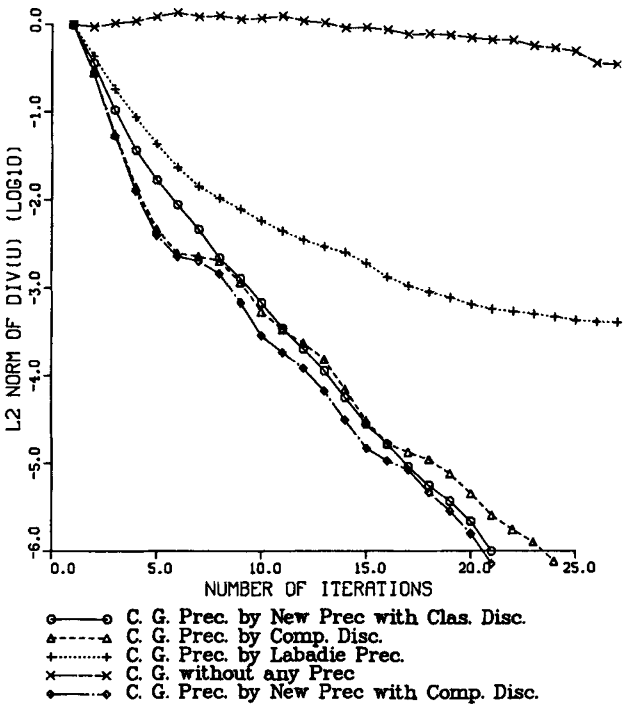

Figure 8. Reduction of the divergence versus the number of iterations for a 3D industrial problem

CONCLUSIONS

We have discussed in this paper some new approaches updating the classical Uzawa methods for solving Stokes equations. These advanced researches have converged on the realization of industrial tools: CEFALO code based on shallow water equations for environmental hydraulics studies[3] and N3S code for Navier–Stokes equations. In both cases these algorithms are compatible with refined turbulence modelling and with other kinds of boundary conditions as detailed in Goussebaile and Jacomy,[19] all these methods satisfying our constraints and permitting an improvement of computation efficiency.

Finally further developments are still under way for taking into account the time variations of diffusion matrices (as in the turbulent case) in the preconditioners through a quasi-Newton approach.[33]

ACKNOWLEDGEMENTS

We are gratefully indebted to Professor R. Glowinski for valuable discussions and encouragement and to Ph. Beque for providing numerical results.

APPENDIX. DISCRETIZED UZAWA ALGORITHM: COMPUTATION ORGANIZATION

Choice of the descent parameter

As explained earlier, Uzawa's algorithm is a gradient method working on the pressure equation. The main iterative process can be written as

$$P_{n+1}=P_n-\rho r_n=P_n-\rho(\mathscr{A}P_n-S)$$

where $\mathscr{A}=BA^{-1}B^{\mathrm{T}}$ and $S=BA^{-1}F$ (with the notation of the numerical results section).

The descent parameter ρ can be chosen positive and small enough or, better, computed in order to minimize at each iteration the residual r_{n+1} in the gradient direction. The optimal value for ρ is explicitly known and depends on the choice of the scalar product generally associated with the operator $\mathscr{A}^i$. The usual choices are the following:

$$\text{Steepest descent}\,(i=-1)\text{:}\ \rho=\frac{(r_n, r_n)}{(\mathscr{A}r_n, r_n)},$$

$$\text{Minimum residual}\,(i=0)\text{:}\quad \rho=\frac{(\mathscr{A}r_n, r_n)}{(\mathscr{A}r_n, \mathscr{A}r_n)}.$$

Implemented algorithm

As described in Fortin and Glowinski,[24] a preconditioned conjugate gradient version of the Uzawa algorithm is used in our codes. In the sequel the computation organization is detailed; C denotes the preconditioner and W the conjugate direction of descent. Let us distinguish the first iteration, which looks like a simple gradient iteration.

Initialize P_0,

First iteration

Step 1. Compute U_0 solving $AU_0=F-B^{\mathrm{T}}P_0$.
Step 2. Compute the residual $R_0=BU_0$.
Step 3. Compute G_0 solving $CG_0=R_0$.
Step 4. Set $W_0=G_0$.
Step 5. Compute Z_0 solving $AZ_0=B^{\mathrm{T}}W_0$.
Step 6. Compute $\rho_0=R_0^{\mathrm{T}}G_0/G_0^{\mathrm{T}}BZ_0$.
Step 7. Compute $P_1=P_0-\rho_0 W_0$.

At this stage the solution of two systems for the velocities is required: one for the right-hand-side contribution (Step 1) and one for the descent parameter (Step 5). For the next iterations one of these solutions can be avoided by taking into account the relation

$$AU_{n+1}=F+B^{\mathrm{T}}P_{n+1}=F+B^{\mathrm{T}}(P_n-\rho_nR_n)=F+B^{\mathrm{T}}P_n-\rho_nB^{\mathrm{T}}R_n,$$
$$AU_{n+1}=AU_n-\rho_nB^{\mathrm{T}}R_n.$$

So we have

$$U_{n+1}=U_n-\rho_nA^{-1}B^{\mathrm{T}}R_n=U_n-\rho_nZ_n, \qquad R_{n+1}=BU_{n+1}=R_n-\rho_nBZ_n.$$

Then it follows:

P_n, U_n, R_n are known.

Iteration $n+1$

```
Step 8.  Compute $G_n$ solving $CG_n=R_n$.
Step 9.  Compute $\lambda_n=R_n^{\mathrm{T}}G_n/R_{n-1}^{\mathrm{T}}G_{n-1}$.
Step 10. Compute $W_n=G_n+\lambda_n W_{n-1}$.
Step 11. Compute $Z_n$ solving $AZ_n=B^{\mathrm{T}}W_n$.
Step 12. Compute $\rho_n=R_n^{\mathrm{T}}G_n/G_n^{\mathrm{T}}BZ_n$.
Step 13. Compute $P_{n+1}$, $U_{n+1}$, $R_{n+1}$:
    $P_{n+1}=P_n-\rho_n W_n$,   $U_{n+1}=U_{n+1}-\rho_nZ_n$,   $R_{n+1}=R_n-\rho_nBZ_n$.
    Go to Step 8 until $\|R_{n+1}\|\leqslant\varepsilon$.
```

Some points have to be emphasized:

(a) The pressure matrix $\mathscr{A}=BA^{-1}B^{\mathrm{T}}$ is never explicitly built during the iterative process.

(b) If the new preconditioner is used, the number of iterations is small enough to avoid some periodic simple gradient iterations related to truncation and round-off errors.

(c) For the velocity system we take advantage of the natural uncoupling of the velocity components and, in order to save CPU time and memory requirements, we solve three smaller systems, one on each velocity component. These three matrices are identical when Dirichlet boundary conditions are used but they can differ if other kinds of boundary conditions are required.

(d) The velocity systems are solved by a conjugate gradient method using an incomplete Choleski decomposition (ICCG method).

(e) If the new preconditioner is used, two linear systems have to be solved: one for the Laplacian, the other for the mass matrix. But the size of the preconditioning systems (number of pressure nodes) is very small compared with the size of the velocity systems. They are solved using a direct solver and are not time-consuming.

(f) As we invert with a direct solver the Laplacian with homogeneous Neumann boundary conditions, we have to take care of its kernel. In our codes a Dirichlet boundary condition is applied on the pressure just for the solution of this system, and the matrix becomes positive definite and symmetrical. Therefore it is necessary to modify the residual in order to obtain a zero mean value field before going on with the mass matrix solution.

REFERENCES*

1. S. Nakazawa, 'Mixed finite element and iterative solution procedure', *Innovative Methods for Non-linear Problems*, Pineridge Press International, London, 1984.

*Note: EDF reports can be obtained from Laboratoire National d' Hydraulique, Research Branch, 6 Quai Watier, 78401 Chatou Cedex, France.

2. A. Hauguel, J. Cahouet, J. Goussebaile and P. Lasbleiz, 'About difficulties raised by a refined turbulence modelling in a Navier–Stokes finite element code', *Seventh Int. Conf. on Computing Methods in Applied Sciences and Engineering*, Versailles, France, 1985.
3. S. Dalsecco, N. Goutal, J. M. Hervouet and Y. Vujasinovic, 'Recent advances in shallow water computations', *Sixth Int. Symp. on Finite Element Methods in Flow Problems*, Antibes, France, 1986.
4. J. Goussebaile, F. Hecht, G. Labadie and L. Reinhart, 'Finite element solution of the shallow water equations by a quasi-direct decomposition procedure', *Int. j. numer. methods fluids*, **4**, 1117–1136 (1984).
5. N. Goutal, 'Résolution des équations de St Venant en régime transcritique par une méthode d'éléments finis: application aux bancs découvrants', *Thèse*, Université Paris VI, 1987.
6. R. Glowinski, J. Goussebaile and G. Labadie, 'Numerical methods for the Stokes problem. Applications to compressible and incompressible viscous flow simulation', in preparation.
7. J. P. Chabard, A. Hauguel and P. Lasbleiz, 'A 3D FEM for turbulent industrial flows', *First World Congress on Computational Mechanics*, Austin, Texas, U.S.A., 1986.
8. R. Peyret and T. D. Taylor, *Computational Methods for Fluid Flow*, Springer Verlag, 1982.
9. J. Cahouet, 'Méthodes de sous-structuration de domaines pour les équations de Navier–Stokes', *EDF Report HE41/85.03*, 1985.
10. J. P. Benque, B. Ibler, A. Keramsi and G. Labadie, 'A finite element method for Navier–Stokes equations', in D. S. H. Norries (ed.), *Proc. Third Int. Conf. on Finite Elements in Flow Problems*, Banff, Alberta, Canada, 10–13 June 1980, vol. 1, pp. 10–120.
11. B. Ibler, 'Resolution des équations de Navier–Stokes par une méthode d'éléments finis', *Thèse de 3eme Cycle*, Université Paris-Sud, 1981; and *EDF Report HE41/81.15*, 1981.
12. A. J. Chorin, 'Numerical solution of incompressible flow problems', *SIAM J. Numer. Anal.*, **2**, 64–71 (1968).
13. R. Temam, *Navier–Stokes Equations*, North-Holland, Amsterdam, 1977.
14. R. Glowinski, *Numerical Methods for Non-Linear Variational Problems*, Springer Verlag, New York, 1984.
15. M. O. Bristeau, R. Glowinski, J. Periaux, P. Perrier, O. Pironneau and G. Poirier, 'Application of the optimal control and finite element methods to the calculation of transonic flows and incompressible flows', *Research Report 78-294*, INRIA, France, 1978.
16. J. Cahouet and A. Hauguel, 'Finite element methods for incompressible Navier–Stokes and for shallow water equations', in *Von Karman Institute Lecture Series*, Rhodes St Genese, Belgium, March 1986; and *EDF Report HE41/86.03*, 1986.
17. V. Girault and P. A. Raviart, 'Finite element approximation of the Navier–Stokes equations', *Lecture Notes in Mathematics*, vol. 749, Springer Verlag, 1979.
18. P. Grisvard, 'Singularités des solutions du problème de Stokes dans un polygone', *Séminaire d'Analyse Numèrique*, Université Paris VI, 1978.
19. J. Goussebaile and A. Jacomy, 'Application a la thermohydraulique des méthodes d'éclatement d'operateurs dans le cadre éléments finis: traitement du modèle k–ε', *EDF Report HE41/85.11*, 1985.
20. C. Bernardi and G. Raugel, 'Methodes Mixtes pour les équations de Navier–Stokes dans un ouvert polygonal plan', *Publication du Laboratoire d'Analyse Numerique, n° 80015*, Universite Paris VI, 1980.
21. D. Serre, 'Invariants des équations de la mécanique. Remarques sur les équations de Navier–Stokes dans 1 cas stationnaire', *Thèse*, Université Paris-Sud, 1982.
22. P. Grisvard, Lectures at Centre de Mathématiques Appliquées, Ecole Polytechnique, 1985 and Universite Paris VI, 1986.
23. K. J. Arrow, L. Hurwicz and H. Uzawa, *Studies in Non-linear Programing*, Stanford University Press, 1958.
24. M. Fortin and R. Glowinski, *Augmented Lagrangian Methods*, North-Holland Amsterdam, 1983.
25. M. Hestenes, 'Multiplier and gradient methods', *J. Optim. Theory Appl.*, **4**, 303–320 (1969).
26. M. J. D. Powell, 'A method for non-linear constraints in minimization problems', in E. Fletcher (ed.), *Minimization*, Academic Press, London, 1969, pp. 238–298.
27. R. Verfurth, 'A combined conjugate gradient multigrid algorithm for the numerical solution of the Stokes problem', *IMA J. Numer. Math.* **4**, 441–455 (1984).
28. R. Verfurth, 'A preconditioned conjugate residual algorithm for the Stokes problem', in R. Braess, W. Hackbusch and U. Trottenberg (eds), *Developments in Multigrid Methods*, Wiley, New York, 1985.
29. Ph. Nigon, 'Une nouvelle classe de méthodes multigrilles pour les problèmes mixtes. Application à la résolution rapide du problème de Stokes', *Thèse*, Ecole Centrale de Lyon, 1984.
30. G. H. Golub and G. A. Meurant, *Resolution Numérique des Grands Systèmes Linèaires*, Eyrolles, Paris, 1983.
31. G. Labadie and P. Lasbleiz, 'Quelques méthodes de résolution du problème de Stokes en éléments finis', *EDF Report HE41/83.01*, 1983.
32. J. Cahouet and J.-P. Chabard, 'Multi-domains and multi-solvers finite element approach for the Stokes problems', in *Innovative Numerical Methods in Engineering*, Springer Verlag, New York, 1986; and *EDF Report HE41/85.27*, 1985.
33. N. Goutal, 'Finite element solution for the transcritical shallow-water equations', to appear in *Mathematical Methods in the Applied Sciences*.
34. J. L. Lions and E. Magenes (eds), *Problèmes aux Limites Homogènes et Applications*, Dunod, Paris, 1968.
35. R. Glowinski and O. Pironneau, 'On a mixed finite element approximation of the Stokes problem', *Numer. Math.* **33**, 397–424 (1979).

36. W. Hackbusch (ed.), 'Multigrid convergence theory', in *Multigrid Methods*, Springer Verlag, Berlin, 1982, pp. 177–219.
37. P. Hood and C. Taylor, 'A numerical solution of the Navier–Stokes equations using the finite element technique', *Comput. Fluids*, **1,** 73–100 (1973).
38. D. Laurence, 'A computation method for the determination of the flow field around vehicles', *Vehicle Aerodynamics* in *Von Karman Institute Lectures Series*, Rhodes St Genese, Belgium, May 1986; and *EDF Report HE41/86.07*, 1986.
39. J. P. Chabard, 'Validation du code éléments finis N3S sur le problème de l'écoulement derriere un cylindre circulaire', *EDF Report HE41/85.23*, 1985.